

# Two years of monitoring supergiant fast X-ray transients with *Swift*

P. Romano,<sup>1\*</sup> V. La Parola,<sup>1</sup> S. Vercellone,<sup>1</sup> G. Cusumano,<sup>1</sup> L. Sidoli,<sup>2</sup>  
H. A. Krimm,<sup>3,4</sup> C. Pagani,<sup>5,6</sup> P. Esposito,<sup>7,8</sup> E. A. Hoversten,<sup>5</sup> J. A. Kennea,<sup>5</sup>  
K. L. Page,<sup>6</sup> D. N. Burrows<sup>5</sup> and N. Gehrels<sup>4</sup>

<sup>1</sup>INAF, Istituto di Astrofisica Spaziale e Fisica Cosmica, Via U. La Malfa 153, I-90146 Palermo, Italy

<sup>2</sup>INAF, Istituto di Astrofisica Spaziale e Fisica Cosmica, Via E. Bassini 15, I-20133 Milano, Italy

<sup>3</sup>NASA/Goddard Space Flight Center, Greenbelt, MD 20771, USA

<sup>4</sup>Universities Space Research Association, Columbia, MD 21044-3432, USA

<sup>5</sup>Department of Astronomy and Astrophysics, Pennsylvania State University, University Park, PA 16802, USA

<sup>6</sup>Department of Physics & Astronomy, University of Leicester, University Road, Leicester LE1 7RH

<sup>7</sup>INAF, Osservatorio Astronomico di Cagliari, località Poggio dei Pini, strada 54, I-09012 Capoterra, Italy

<sup>8</sup>Istituto Nazionale di Fisica Nucleare, sezione di Pavia, via A. Bassi 6, I-27100 Pavia, Italy

Accepted 2010 August 18. Received 2010 August 17; in original form 2010 March 17

## ABSTRACT

We present results based on 2 yr of intense *Swift* monitoring of three supergiant fast X-ray transients (SFXTs), IGR J16479–4514, XTE J1739–302 and IGR J17544–2619, which we started in 2007 October. Our out-of-outburst intensity-based X-ray (0.3–10 keV) spectroscopy yields absorbed power laws characterized by hard photon indices ( $\Gamma \sim 1-2$ ). The broad-band (0.3–150 keV) spectra of these sources, obtained while they were undergoing new outbursts observed during the second year of monitoring, can be fitted well with models typically used to describe the X-ray emission from accreting neutron stars in high-mass X-ray binaries. We obtain an assessment of how long each source spends in each state using a systematic monitoring with a sensitive instrument. By considering our monitoring as a casual sampling of the X-ray light curves, we can infer that the time these sources spend in bright outbursts is between 3 and 5 per cent of the total. The most probable X-ray flux for these sources is  $\sim(1-2) \times 10^{-11} \text{ erg cm}^{-2} \text{ s}^{-1}$  (2–10 keV, unabsorbed), corresponding to luminosities of the order of a few  $10^{33}$  to a few  $10^{34} \text{ erg s}^{-1}$  (two orders of magnitude lower than the bright outbursts). In particular, the duty-cycle of *inactivity* is  $\sim 19, 39$  and  $55$  per cent ( $\sim 5$  per cent uncertainty) for IGR J16479–4514, XTE J1739–302 and IGR J17544–2619, respectively. We present a complete list of BAT onboard detections, which further confirm the continued activity of these sources. This demonstrates that true quiescence is a rare state and that these transients accrete matter throughout their life at different rates. Variability in the X-ray flux is observed at all time-scales and intensity ranges we can probe. Superimposed on the day-to-day variability is intraday flaring, which involves flux variations up to one order of magnitude that can occur down to time-scales as short as  $\sim 1$  ks, and which can be naturally explained by the accretion of single clumps composing the donor wind with masses  $M_{\text{cl}} \sim (0.3-2) \times 10^{19} \text{ g}$ . Thanks to the *Swift* observations, the general picture we obtain is that, despite individual differences, common X-ray characteristics of this class are now well defined, such as outburst lengths well in excess of hours, with a multiple peaked structure, and a high dynamic range (including bright outbursts), up to approximately four orders of magnitude.

**Key words:** X-rays: binaries – X-rays: individual: IGR J16479–4514 – X-rays: individual: XTE J1739–302 – X-rays: individual: IGR J17544–2619.

## 1 INTRODUCTION

Supergiant fast X-ray transients (SFXTs) constitute a new class of high-mass X-ray binaries (HMXBs). Discovered by *INTEGRAL*

\*E-mail: romano@ifc.inaf.it

(Sguera et al. 2005), they are firmly associated with OB supergiant stars via optical spectroscopy, and display sporadic X-ray outbursts significantly shorter than those of typical Be/X-ray binaries, characterized (as observed by *INTEGRAL*/IBIS) by bright flares (peak luminosities of  $10^{36}$ – $10^{37}$  erg s $^{-1}$ ) lasting for a few hours (Sguera et al. 2005; Negueruela et al. 2006). The quiescence, which is characterized by a soft spectrum (likely thermal), shows a luminosity of  $\sim 10^{32}$  erg s $^{-1}$  so that SFXTs display a dynamic range of three to five orders of magnitude. Their hard X-ray spectra during outburst resemble those of HMXBs hosting accreting neutron stars, with hard power laws below 10 keV combined with high energy cut-offs at  $\sim 15$ –30 keV, sometimes strongly absorbed at soft energies (Sidoli, Paizis & Mereghetti 2006; Walter et al. 2006). Therefore, it is tempting to assume that all SFXTs might host a neutron star, even if pulse periods have only been measured for a few SFXTs. Consensus has not been reached yet on the actual mechanism producing the outbursts, but it is probably related to either the properties of the wind from the supergiant companion (in’t Zand 2005; Sidoli et al. 2007; Walter & Zurita Heras 2007; Negueruela et al. 2008) or the presence of gated mechanisms (Bozzo, Falanga & Stella 2008a).

*Swift* is currently the only observatory which, thanks to its unique fast-slewing capability and its broad-band energy coverage, can catch outbursts from these fast transients in their very early stages and study them panchromatically as they evolve, thus providing invaluable information on the nature of the mechanisms producing them.

Furthermore, thanks to its flexible observing scheduling, which makes a monitoring effort cost-effective, *Swift* has given SFXTs the first non-serendipitous attention through monitoring campaigns that cover all phases of their lives with a high sensitivity in the soft X-ray regime, where most SFXTs had not been observed before (Romano et al. 2009b, hereinafter Paper V).

In our previous papers of this series, we described the long-term X-ray emission outside the bright outbursts based on the first 4 months’ data (Sidoli et al. 2008b, hereinafter Paper I), the outbursts of IGR J16479–4514 (Romano et al. 2008d, hereinafter Paper II; Paper V) and the prototypical IGR J17544–2619 and XTE J17391–302 (Sidoli et al. 2009c, hereinafter Paper III; Sidoli et al. 2009a, hereinafter Paper IV).

In this paper, we continue our characterization of the long term properties of our sample as derived from a 2-yr-long high-sensitivity X-ray coverage. We report on the new X-ray Telescope (XRT, Burrows et al. 2005) and the UV/Optical Telescope (UVOT, Roming et al. 2005) data collected in 2009 between January 29 and November 3 and we exploit the longer baseline for in-depth soft X-ray spectral analysis. Furthermore, we show our results on the outbursts caught by the Burst Alert Telescope (BAT, Barthelmy et al. 2005) during the second year of our monitoring campaign, as well as the BAT onboard triggers registered during 2009.

## 2 SAMPLE AND OBSERVATIONS

During the second year of *Swift* observations, we monitored three targets, XTE J1739–302, IGR J17544–2619 and IGR J16479–4514.

XTE J1739–302 was discovered in 1997 August by *RXTE* (Smith et al. 1998), when it reached a peak flux of  $3.6 \times 10^{-9}$  erg cm $^{-2}$  s $^{-1}$  (2–25 keV) and has a long history of flaring activity recorded by *INTEGRAL* (Sguera et al. 2006; Walter & Zurita Heras 2007; Blay et al. 2008) and by *Swift* (Paper III; Paper IV). Recently, Drave et al. (2010) reported the discovery of a  $51.47 \pm 0.02$  d orbital period based

on  $\sim 12.4$  Ms of *INTEGRAL* data. The optical counterpart is an O8I star (Negueruela et al. 2006).

The first recorded flare from IGR J17544–2619 was observed by *INTEGRAL* in 2003 (Sunyaev et al. 2003), when the source reached a flux of 160 mCrab (18–25 keV). Several more flares, lasting up to 10 h, were detected by *INTEGRAL* in the following years (Grebenev, Lutovinov & Sunyaev 2003; Grebenev et al. 2004; Sguera et al. 2006; Kuulkers et al. 2007; Walter & Zurita Heras 2007) with fluxes up to 400 mCrab (20–40 keV) and some were found in archival *BeppoSAX* observations (in’t Zand et al. 2004). Subsequent flares were observed by *Swift* (Krimm et al. 2007; Paper III; Paper IV) and *Suzaku* (Rampy, Smith & Negueruela 2009). Recently, Clark et al. (2009) reported the discovery of a  $4.926 \pm 0.0001$  d orbital period based on the  $\sim 4.5$  yr of *INTEGRAL* data. The optical counterpart is an O9Ib star (Pellizza, Chaty & Negueruela 2006).

IGR J16479–4514 was discovered by *INTEGRAL* in 2003 (Molkov et al. 2003), during an outburst that reached the flux level of  $\sim 12$  mCrab (18–25 keV). Since then the source has shown frequent flaring activity, recorded by both *INTEGRAL* (Sguera et al. 2005, 2006; Walter & Zurita Heras 2007) and *Swift* (Kennea et al. 2005; Markwardt & Krimm 2006; Paper II; Bozzo et al. 2009; Paper V), which led to its inclusion in the SFXT class. The optical counterpart is an O8.5I star (Rahoui et al. 2008). Recently, Bozzo et al. (2008b) reported an episode of sudden obscuration in a long *XMM-Newton* observation obtained after the 2009 March 19 outburst, possibly an X-ray eclipse by the supergiant companion. This was later confirmed by Jain, Paul & Dutta (2009), who discovered a 3.32 d orbital period in the first 4 yr of BAT data and *RXTE*/ASM data, and by Paper V by using XRT observations spanning 1 yr.

We monitored the first two targets as they are generally considered prototypical SFXTs and the latter because of its frequent triggering of the BAT since the beginning of the mission. We planned two observations per week per object (IGR J16479–4514 and IGR J17544–2619) and three observations per week per object (XTE J1739–302), each 1 ks long. The observation logs are reported in Tables 1–3. This strategy was chosen to fit within the regular observing schedule of the main observing targets for *Swift*, gamma-ray bursts (GRBs).

Furthermore, in order to ensure simultaneous narrow field instrument (NFI) data, the *Swift* Team enabled automatic rapid slews to these objects following detection of flares by the BAT, in the same fashion as is currently done for GRBs. During the campaign, we often requested target of opportunity (ToO) observations whenever one of the sources showed interesting activity or following outbursts to better monitor the decay of the XRT light curve, thus obtaining a finer sampling of the light curves and allowing us to study all phases of the evolution of an outburst.

During the second year (2009), we collected a total of 228 *Swift* observations as part of our programme, for a total net XRT exposure of  $\sim 243$  ks accumulated on all sources and distributed as shown in Table 4.

## 3 DATA REDUCTION

The XRT data were uniformly processed with standard procedures (*XRTPIPELINE* v0.12.3), and filtering and screening criteria by using *FTOOLS* in the *HEASOFT* package (v6.7). We considered both windowed-timing (WT) and photon-counting (PC) mode data, and selected event grades 0–2 and 0–12, respectively (Burrows et al. 2005). When appropriate, we corrected for pile-up by determining the size of the affected core of the point spread function (PSF) by comparing the observed and nominal PSF (Vaughan et al. 2006),

**Table 1.** Observation log for IGR J16479–4514. The full table is available online (see Supporting Information).

Sequence	Instrument/mode	Start time (UT) (yyyy-mm-dd hh:mm:ss)	End time (UT) (yyyy-mm-dd hh:mm:ss)	Net exposure (s)
00030296096	XRT/PC	2009-02-19 21:23:39	2009-02-19 23:11:56	1178
00030296097	XRT/PC	2009-02-23 15:15:37	2009-02-23 17:08:58	1925
00030296098	XRT/PC	2009-02-26 20:38:22	2009-02-26 22:21:58	902
00030296099	XRT/PC	2009-03-01 01:36:58	2009-03-01 03:20:57	1014
00030296101	XRT/PC	2009-03-08 01:58:11	2009-03-08 02:11:58	813

**Table 2.** Observation log for IGR J17391–3021. The full table is available online (see Supporting Information).

Sequence	Instrument/mode	Start time (UT) (yyyy-mm-dd hh:mm:ss)	End time (UT) (yyyy-mm-dd hh:mm:ss)	Net exposure (s)
00030987098	XRT/PC	2009-02-21 13:32:13	2009-02-21 15:19:57	1382
00030987099	XRT/PC	2009-02-23 07:26:20	2009-02-23 09:11:58	1354
00030987100	XRT/PC	2009-02-25 14:13:53	2009-02-25 15:56:58	1123
00030987101	XRT/PC	2009-02-27 23:51:23	2009-02-27 23:59:44	487
00030987102	XRT/PC	2009-03-02 01:42:07	2009-03-02 01:57:57	939

**Table 3.** Observation log for IGR J17544–2619. The full table is available online (see Supporting Information).

Sequence	Instrument/mode	Start time (UT) (yyyy-mm-dd hh:mm:ss)	End time (UT) (yyyy-mm-dd hh:mm:ss)	Net exposure (s)
00035056083	XRT/PC	2009-02-21 16:45:15	2009-02-21 18:32:57	1387
00035056084	XRT/PC	2009-02-24 07:31:27	2009-02-24 07:50:58	1160
00035056085	XRT/PC	2009-02-28 01:28:32	2009-02-28 01:45:57	1034
00035056086	XRT/PC	2009-03-03 19:35:54	2009-03-03 21:18:57	784
00035056087	XRT/PC	2009-03-07 20:03:32	2009-03-07 21:41:56	268

**Table 4.** Summary of the *Swift*/XRT monitoring campaign.

Name	Campaign Start (yyyy-mm-dd)	Campaign End (yyyy-mm-dd)	$N^a$	Exposure <sup>b</sup> (ks)	Outburst dates <sup>c</sup> (yyyy-mm-dd)	BAT trigger	Reference
IGR J16479–4514	2007-10-26	2008-10-25	70	75.2	2008-03-19 2008-05-21	306829 312068	<i>Romano et al. (2008d)</i>
	2009-01-29	2009-10-25	74	85.7	2009-01-29	341452	Romano et al. (2009e), La Parola et al. (2009)
XTE J1739–302	2007-10-27	2008-10-31	95	116.1	2008-04-08 2008-08-13	308797 319963	<i>Romano et al. (2008c)</i> , <i>Sidoli et al. (2009c)</i> <i>Romano et al. (2008b)</i> , <i>Sidoli et al. (2009a)</i>
	2009-02-21	2009-11-01	89	89.6	2009-03-10	346069	Romano et al. (2009d), this work
IGR J17544–2619	2007-10-28	2008-10-31	77	74.8	2007-11-08 2008-03-31	BTM 308224	<i>Krimm et al. (2007)</i> <i>Sidoli et al. (2008a,c)</i>
	2009-02-21	2009-11-03	65	68.0	2008-09-04	XM	<i>Romano et al. (2008a)</i> , <i>Sidoli et al. (2009a)</i> , this work
					2009-03-15 2009-06-06	BTM 354221	Krimm, Romano & Sidoli (2009), this work Romano et al. (2009f), this work
First year			330	362.6			
Second year			228	243.3			
Total			558	605.9			

<sup>a</sup>Number of observations (individual ObsIDs) obtained during the monitoring campaign.

<sup>b</sup>*Swift*/XRT net exposure.

<sup>c</sup>BAT trigger dates. BTM = triggered the BAT Transient Monitor; XM = discovered in XRT monitoring data.

Note. We report the data from the first year in italics.

and excluding from the analysis all the events that fell within that region. We used the latest spectral redistribution matrices in CALDB (20091130).

The BAT data of the outbursts (see Section 5) were analysed using the standard BAT software within FTOOLS. Mask-tagged

BAT light curves were created in the standard energy bands, and rebinned to fulfil at least one of the following conditions, achieving a signal-to-noise ratio (S/N) of 5 or bin length of 100 s. Response matrices were generated with BATDRMGEN using the latest spectral redistribution matrices. For this paper, we also considered the BAT

Transient Monitor data (Krimm et al. 2006, 2008),<sup>1</sup> covering the same time-interval as the NFI pointed observations. The data were rebinned to a 4-d resolution to ensure a larger number of detections and to closely match the NFI sampling.

The UVOT observed the three targets simultaneously with the XRT. The data of XTE J1739–302 and IGR J16479–4514 were taken in general with the ‘Filter of the Day’ (FoD), that is, the filter chosen for all observations to be carried out during a specific day in order to minimize the filter wheel rotation (*u, uvw1, uvw2* and *uvm2*), while IGR J17544–2619 was only observed with UVOT from 2009-06-06 to 2009-09-30, in the *uvw1* and *v* filters, and in FoD for the remainder of the campaign. However, during the outbursts on 2009-03-10 of XTE J1739–302 and on 2009-06-06 of IGR J17544–2619, all filters were used in the typical GRB sequence (Roming et al. 2005). The data analysis was performed using the `UVOTSUM` and `UVOTSOURCE` tasks included in the `FTOOLS` software. The latter task calculates the magnitude through aperture photometry within a circular region and applies specific corrections due to the detector characteristics. The reported magnitudes are on the UVOT photometric system described in Poole et al. (2008) and are not corrected for Galactic extinction. At the position of IGR J16479–4514, no detection was achieved down to a  $3\sigma$  limit of  $u = 21.27$  mag.

All quoted uncertainties are given at 90 per cent confidence level for one interesting parameter, unless otherwise stated. The spectral indices are parametrized as  $F_\nu \propto \nu^{-\alpha}$ , where  $F_\nu$  ( $\text{erg cm}^{-2} \text{s}^{-1} \text{Hz}^{-1}$ ) is the flux density as a function of frequency  $\nu$ ; we adopt  $\Gamma = \alpha + 1$  as the photon index,  $N(E) \propto E^{-\Gamma}$  ( $\text{photon cm}^{-2} \text{s}^{-1} \text{keV}^{-1}$ ).

## 4 TIMING

### 4.1 XRT light curves and inactivity duty-cycle

The 0.2–10 keV XRT light curves collected from 2007 October 26 to 2009 November 3 are shown in Fig. 1. They are corrected for pile-up, PSF losses and vignetting, and background-subtracted. Each point in the light curves refers to the average flux observed during each observation performed with XRT; the exceptions are the outbursts (listed in Table 4), where the data were binned to include at least 20 source counts per time-bin to best represent the count rate dynamical range.

One of our goals is to calculate the percentage of time each source spent in each flux state. We consider our monitoring as a casual sampling of the light curve at a resolution of  $\sim 3$ –4 d over a  $> 2$  yr baseline. We considered the following three states: (i) BAT-detected outburst; (ii) intermediate state (all observations yielding a firm detection, excluding outburst ones); and (iii) ‘non-detections’ (detections with a significance below  $3\sigma$ ). From the latter state, we excluded all observations that had a net exposure below 900 s [corresponding to 2–10 keV flux limits that vary between 1 and  $3 \times 10^{-12} \text{ erg cm}^{-2} \text{ s}^{-1}$  ( $3\sigma$ ), depending on the source, see Paper V]. This was done because *Swift* is a GRB-chasing mission and several observations were interrupted by GRB events; therefore, the consequent non-detection may be due to the short exposure and not, exclusively, due to the source being faint.

The duty-cycle of *inactivity* is defined (Paper V) as the time each source spends *undetected* down to a flux limit of  $(1-3) \times$

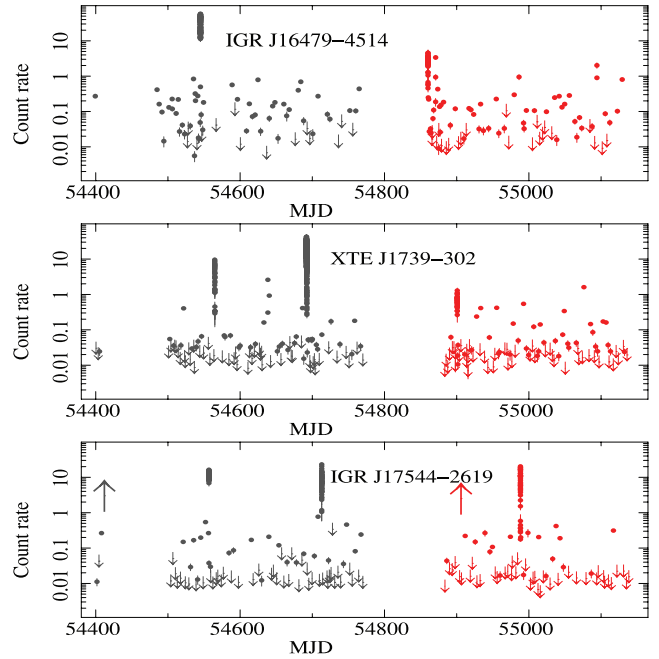


**Figure 1.** *Swift*/XRT (0.2–10 keV) light curves. The data were collected from 2007 October 26 to 2008 November 15 (first year, grey) and from 2009 January 29 to November 3 (second year, red). The downward-pointing arrows are  $3\sigma$  upper limits. The upward pointing arrows mark flares that triggered the BAT Transient Monitor on MJD 544 14 and 549 06. Data up to MJD  $\sim 547$  70 (grey) were published in Paper V.

$10^{-12} \text{ erg cm}^{-2} \text{ s}^{-1}$ :

$$\text{IDC} = \Delta T_\Sigma / [\Delta T_{\text{tot}} (1 - P_{\text{short}})], \quad (1)$$

where  $\Delta T_\Sigma$  is sum of the exposures accumulated in all observations, each in excess of 900 s, where only a  $3\sigma$  upper limit was achieved (Table 5, column 2),  $\Delta T_{\text{tot}}$  is the total exposure accumulated (Table 4, column 5) and  $P_{\text{short}}$  is the percentage of time lost to short observations (exposure  $< 900$  s, Table 5, column 3). We obtain IDC = 19, 39 and 55 per cent for IGR J16479–4514, XTE J1739–302 and IGR J17544–2619, respectively (Table 5, column 4), with an estimated error of  $\sim 5$  per cent. We note that these values are based on the whole 2-yr campaign and that the IDC calculated with the observations of 2009 only is 21, 39 and 55 per cent. Finally, as we can consider our monitoring as a casual sampling of the light curve, we can also infer that the time these sources spend in bright outbursts is between 3 and 5 per cent of the total (estimated error of  $\sim 5$  per cent).

**Table 5.** Duty-cycle of inactivity of the three SFXTs (2-yr campaign).

Name	$\Delta T_\Sigma$ (ks)	$P_{\text{short}}$ (per cent)	IDC (per cent)	Rate $_{\Delta T_\Sigma}$ ( $10^{-3} \text{ counts s}^{-1}$ )
IGR J16479–4514	29.7	3	19	$3.1 \pm 0.5$
XTE J1739–302	71.5	10	39	$4.0 \pm 0.3$
IGR J17544–2619	69.3	10	55	$2.2 \pm 0.2$

Count rates are in units of  $10^{-3} \text{ counts s}^{-1}$  in the 0.2–10 keV energy band.  $\Delta T_\Sigma$  is sum of the exposures accumulated in all observations, each in excess of 900 s, where only a  $3\sigma$  upper limit was achieved;  $P_{\text{short}}$  is the percentage of time lost to short observations; IDC is the duty-cycle of *inactivity*, that is, the time each source spends undetected down to a flux limit of  $(1-3) \times 10^{-12} \text{ erg cm}^{-2} \text{ s}^{-1}$ ; and Rate $_{\Delta T_\Sigma}$  is detailed in the text (Section 6).

<sup>1</sup> <http://swift.gsfc.nasa.gov/docs/swift/results/transients/>

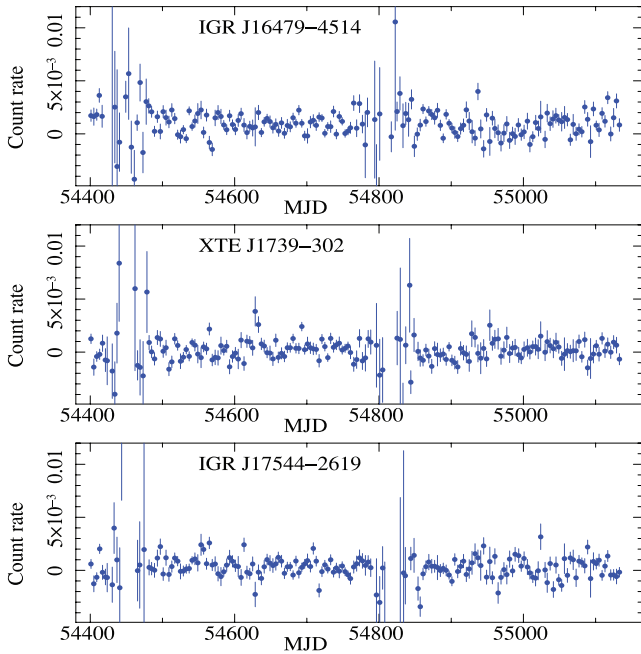


**Figure 2.** *Swift*/BAT Transient Monitor light curves in the 15–50 keV energy range in units of counts s<sup>−1</sup> cm<sup>−2</sup>.

#### 4.2 BAT transient monitor data and onboard detections

The 15–50 keV BAT Transient Monitor light curves collected from 2007 October 26 to 2009 November 3 are shown in Fig. 2, rebinned at a 4-d resolution. The two gaps in each of the BAT light curves preceded and followed by points with large error bars are an artefact of *Swift*'s Sun-avoidance pointing strategy. When the sources are near the Sun, they will be found only at the edges of the BAT FOV, where the sensitivity is reduced and for a few weeks each year, the sources cannot be observed at all.

In Table 6, we report the BAT onboard detections in the 15–50 keV band. If an alert was generated, a BAT trigger was assigned (Column 4) and notices were disseminated.<sup>2</sup> For some of these triggers, a burst response (slew and repointing of the NFI) was also initiated, depending on GRB observing load, observing constraints and interest in the sources. More details on several of these triggers can be found in the papers of our series (see Table 4 for references). The combination of all these data shows how active the sources are outside the bright outbursts when observed by the BAT.

#### 4.3 UVOT light curves

The UVOT performed observations simultaneously with the XRT, throughout most of the *Swift*/XRT monitoring of the SFXTs. Figs 3(a) and (b) show the UVOT *u* and *uvw1* light curves of XTE J1739–302 of the whole campaign. The dashed vertical lines mark the X-ray outbursts. The *u* and *uvw1* magnitudes show variability of marginal statistical significance; a fit against a constant yields  $\chi^2_\nu(u) = 2.13$  for 45 degrees of freedom (d.o.f.), null hypothesis probability (nhp) =  $1.5 \times 10^{-5}$  ( $\sim 4\sigma$ ) and  $\chi^2_\nu(uvw1) = 2.18$  for 20 d.o.f., nhp =  $1.6 \times 10^{-3}$  ( $\sim 3\sigma$ ). The *uvw2* magnitudes are mostly upper limits, and the five detections yield a mean of  $uvw2 = 20.42 \pm 0.14$  mag. In Paper V, we reported a marginally

**Table 6.** BAT onboard detections in the 15–50 keV band during 2009.

MJD	Date	Time <sup>a</sup>	BAT trigger number <sup>b</sup>	S/N <sup>c</sup>
IGR J16479–4514				
548 60	2009-01-29	06:32:06–06:48:1	341452 (NFI)	10.68
548 95	2009-03-04	17:43:07–18:13:47		
549 15	2009-03-25	00:13:07		
549 58	2009-05-06	19:06:51		
549 86	2009-06-03	23:45:07		
550 79	2009-09-05	00:09:35		
551 16	2009-10-12	03:25:31–03:47:39		
XTE J1739–302				
549 01	2009-03-10	18:18:35–18:45:15	346069 (NFI) <sup>d</sup>	6.81
550 79	2009-09-05	05:00:27		
551 07	2009-10-03	01:07:15–01:16:51		
IGR J17544–2619				
549 45	2009-04-24	11:19:15		
549 88	2009-06-06	07:49:00	354221 (NFI) <sup>e</sup>	8.15
550 02	2009-06-20	02:45:39		
550 24	2009-07-12	10:59:55		
550 63	2009-08-20	03:16:43		
550 74	2009-08-30	12:33:55		
551 32	2009-10-28	19:24:11		

<sup>a</sup>Time of the start of the BAT trigger or the time-range when onboard detections were obtained.

<sup>b</sup>BAT regular trigger, as was disseminated through GCNs. NFI indicates that there are data from the narrow-field instrument.

<sup>c</sup>Onboard image significance in units of  $\sigma$ .

<sup>d</sup>This work, Section 5.1.

<sup>e</sup>This work, Section 5.2.

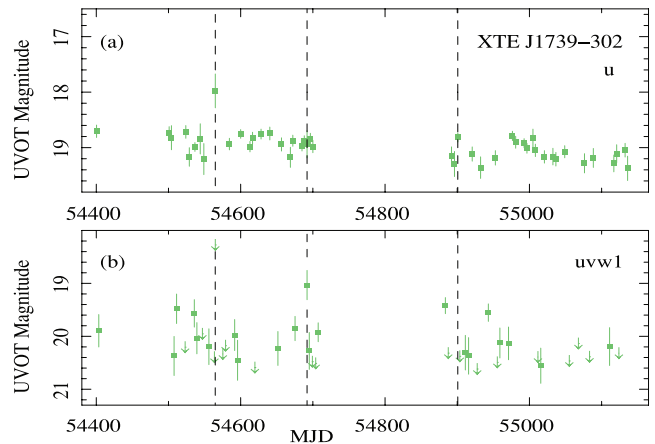


**Figure 3.** UVOT light curves of XTE J1739–302. The filters used are indicated in each panel. The vertical dashed lines mark the BAT outbursts.

significant ( $2\text{--}3\sigma$ ) increase in the *u* magnitude during the first recorded outburst of this source (2008-04-08, MJD 54565), while during the second outburst (2008-08-13, MJD 54692), the *u* magnitude is consistent with the mean for the whole campaign. The third reported outburst (2009-03-10, MJD 549 01), like the second, shows no variation of the *u* magnitude, with respect to the mean of the campaign. Observations were also taken once in the *v* and *b* filters during 2009 as a follow-up ToO (ObsID 00030987132), where we measure  $v = 15.25 \pm 0.03$  and  $b = 18.21 \pm 0.07$  mag. Both values are consistent with the ones obtained during and away from outbursts.

<sup>2</sup> [http://gcn.gsfc.nasa.gov/gcn/swift\\_grbs.html](http://gcn.gsfc.nasa.gov/gcn/swift_grbs.html)

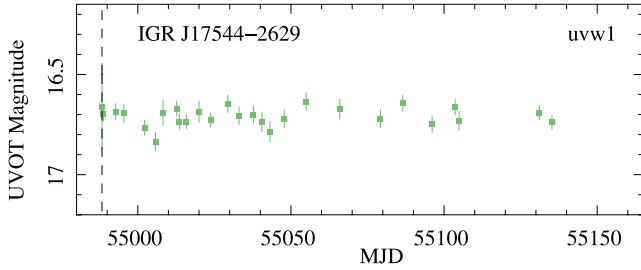


**Figure 4.** UVOT *uvw1* light curve of IGR J17544–2619. The vertical dashed lines mark the BAT outbursts.

In Fig. 4, we show the UVOT *uvw1* light curve of IGR J17544–2619. It is remarkably stable, as a fit against a constant yields  $\chi^2_{\nu}(uvw1) = 1.08$  for 26 d.o.f.,  $\text{nhp}=0.35$ . There are also a few observations performed in the other filters. We obtain  $uvm2 = 20.3 \pm 0.3$ ,  $20.0 \pm 0.3$ ,  $19.9 \pm 0.2$  and  $19.9 \pm 0.3$  mag (ObsID 00035056089, 00035056141, 00035056142 and 00035056148, respectively),  $uvw2 = 18.16 \pm 0.06$  and  $18.05 \pm 0.06$  mag (ObsID 00035056143 and 00035056144, respectively), and  $u = 15.25 \pm 0.09$  mag (ObsID 00035056145). During the 2009 June 6 outburst (ObsID 354221000, MJD 549 88), all filters were used. The observed magnitudes are  $u = 15.16 \pm 0.01$  mag,  $b = 14.55 \pm 0.04$  mag and  $uvw1 = 16.7 \pm 0.2$  mag. The *uvw1* value is consistent with those obtained during the remainder of the campaign. The  $b$  magnitude is very close to the coincidence limit, thus heavily corrected for coincidence loss.

## 5 OUTBURSTS IN 2009

The year 2009 opened with the outburst of IGR J16479–4514 on January 29, which we reported in Paper V. Here, we analyse the data from three more outbursts caught from the sources in our sample.

### 5.1 IGR J17391–3021

XTE J1739–302 triggered the BAT on 2009 March 10 at 18:39:55 UT (image trigger = 346069). We report the BAT light curve in the 15–25 keV band in Fig. 5. The time-averaged spectrum ( $T+0.0$  to  $T+320.0$  s) is best fitted by a simple power-law model with a photon index of  $2.8^{+0.8}_{-0.6}$ , and the 15–50 keV flux is  $7.6 \times 10^{-10}$  erg cm<sup>2</sup> s<sup>-1</sup>. *Swift* did not slew immediately in response to this trigger, so no NFI data were collected simultaneously with the BAT data. Observation 00030987107 (1.9 ks net exposure, see Table 2) was obtained as a high-priority ToO observation, instead. The light curve obtained between  $T+5257$  and  $T+10\,538$  s, since

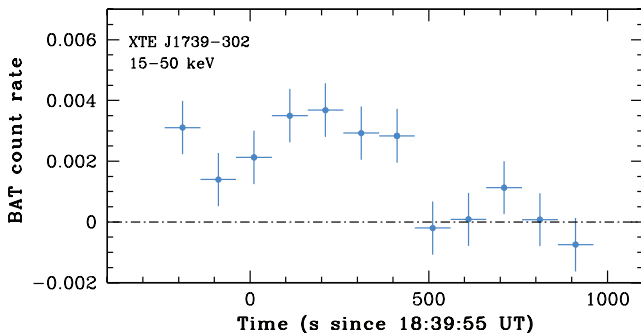


**Figure 5.** BAT light curve in the 15–50 keV band of the 2009 March 10 outburst of XTE J1739–302, in units of counts s<sup>-1</sup> det<sup>-1</sup>.

the trigger shows a mean count rate of 0.4–1 counts s<sup>-1</sup>. The mean XRT/PC spectrum can be fitted with an absorbed power law with a photon index of  $\Gamma = 1.1 \pm 0.4$  and an absorbing column density of  $N_{\text{H}} = (3 \pm 1) \times 10^{22}$  cm<sup>-2</sup> ( $\chi^2_{\nu} = 1.1$  for 25 d.o.f.). The mean unabsorbed 2–10 keV flux is  $9 \times 10^{-11}$  erg cm<sup>2</sup> s<sup>-1</sup>, which translates into a luminosity of  $7 \times 10^{34}$  erg s<sup>-1</sup> (assuming a distance of 2.7 kpc, Rahoui et al. 2008). Further ToO observations were performed on 2009 March 11 (ObsID 00030987108 and 00030987109 in Table 2), when the XRT count rate was down to a few 10<sup>-2</sup> counts s<sup>-1</sup>. These spectral results are in general agreement with those obtained during previous outbursts, both in terms of hard photon index and in terms of a relatively lower column density (comparable with the out-of-outburst values).

### 5.2 IGR J17544–2619

Two outbursts of IGR J17544–2619 were caught during 2009. The first was observed by the BAT Transient Monitor as a sequence of bright flares. In the *Swift* pointings starting at 2009-03-15 23:52:40 UT (1024 s exposure) and at 2009-03-16 01:27:36 UT (1152 s), the source reached  $0.026 \pm 0.005$  counts s<sup>-1</sup> cm<sup>-2</sup> (115 mCrab, 15–50 keV band) and  $0.032 \pm 0.005$  counts s<sup>-1</sup> cm<sup>-2</sup> (140 mCrab), respectively. It then faded below detectability before re-brightening twice more on 2009 March 16: 95 mCrab in a 1152-s exposure beginning at 06:16:40 UT and then to 85 mCrab in a 384-s exposure beginning at 09:25:52 UT. XRT observations were performed as part of our regular monitoring on 2009 March 14 (see Table 3),  $\sim 46$  h before the BAT outburst. A  $3\sigma$  upper limit was obtained at  $1.6 \times 10^{-2}$  counts s<sup>-1</sup>. A later observation, obtained as a ToO on 2009 March 16 ( $\sim 16$  h after the outburst), yielded a  $3\sigma$  upper limit at  $1.3 \times 10^{-2}$  counts s<sup>-1</sup>.

IGR J17544–2619 triggered the BAT on 2009 June 6 at 07:48:59 UT (image trigger = 354221). *Swift* immediately slewed to the target, so that the NFIs started observing about 164 s after the trigger. Fig. 6 shows the XRT and BAT light curves, where it must be noted

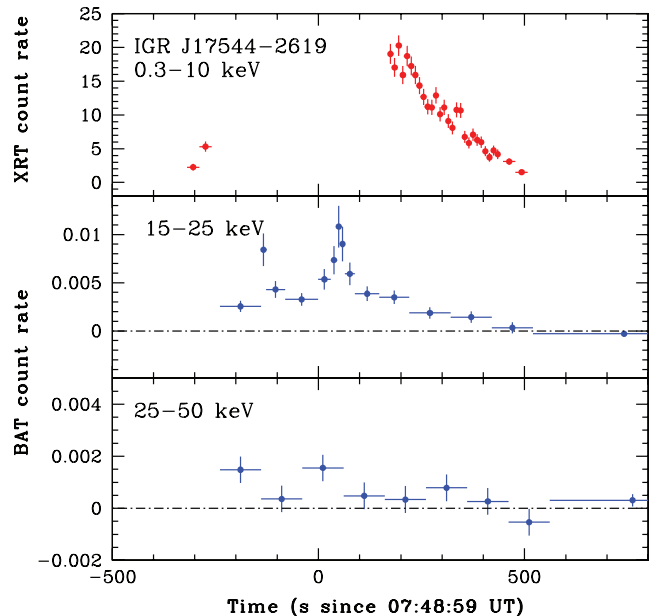


**Figure 6.** Light curves of the 2009 June 6 outburst of IGR J17544–2619. The XRT data preceding the outburst were collected as a pointed observation, part of our monitoring programme. The BAT data are in units of counts s<sup>-1</sup> det<sup>-1</sup>.

that the first two XRT points, preceding the outburst, were collected as a pointed observation, part of our monitoring programme. The initial XRT burst data (WT mode in ObsID 00354221000, see Table 3, 170–446 s since the trigger) show a decaying light curve with a count rate that started at about 20 counts  $s^{-1}$ . The following PC data (448–538 s) seamlessly continue the decaying

**Table 7.** Spectral fits of simultaneous XRT and BAT data of IGR J17544–2619 during the 2009 June 6 outburst.

Model	$N_H^a$	$\Gamma$	$E_c$	$E_f$	Flux <sup>c</sup>	$\chi^2_v$ /d.o.f.
POW <sup>b</sup>	$2.2^{+0.3}_{-0.2}$	$1.7^{+0.1}_{-0.1}$			2.6	1.53/117
HCT <sup>b</sup>	$1.0^{+0.2}_{-0.3}$	$0.6^{+0.2}_{-0.4}$	$3^{+1}_{-1}$	$8^{+4}_{-3}$	1.9	0.92/115
CPL <sup>b</sup>	$1.0^{+0.3}_{-0.2}$	$0.4^{+0.3}_{-0.3}$	$7^{+4}_{-2}$		1.9	0.94/116

<sup>a</sup>Absorbing column density in units of  $10^{22} \text{ cm}^{-2}$ .

<sup>b</sup>POW = simple absorbed power law; HCT = absorbed power law with high energy cut-off  $E_c$  (keV) and e-folding energy  $E_f$  (keV); and CPL = cut-off power law with energy cut-off  $E_c$  (keV).

<sup>c</sup>Unabsorbed 0.5–100 keV flux in units of  $10^{-9} \text{ erg cm}^{-2} \text{ s}^{-1}$ .

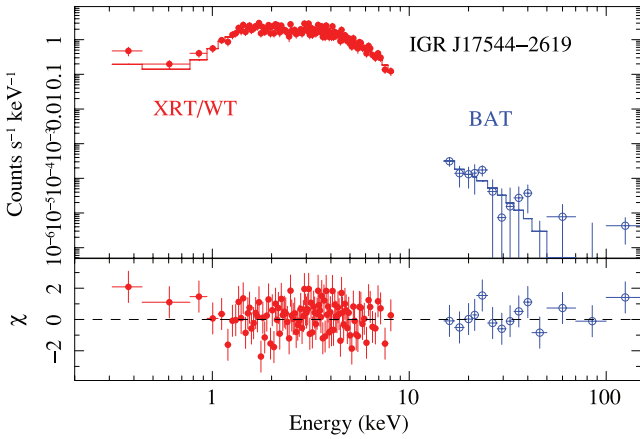


**Figure 7.** Spectroscopy of the 2009 June 6 outburst of IGR J17544–2619. Top panel: data from the XRT/WT spectrum and simultaneous BAT spectrum fitted with a CUTOFFPL model. Bottom panel: residuals in units of standard deviations.

**Table 8.** XRT spectroscopy of the three SFXTs (2007–2009 data set).

Name	Spectrum	Rate (counts $s^{-1}$ )	$N_H$ ( $10^{22} \text{ cm}^{-2}$ )	Parameter $\Gamma$	Flux <sup>a</sup> (2–10 keV)	Luminosity <sup>b</sup> (2–10 keV)	$\chi^2_v$ /d.o.f. <sup>c</sup> C-stat (per cent)
IGR J16479–4514	High	>0.55	$8.2^{+0.8}_{-0.7}$	$1.1^{+0.2}_{-0.2}$	120	5	1.2/193
	Medium	[0.22–0.55]	$8.6^{+0.8}_{-0.8}$	$1.3^{+0.2}_{-0.2}$	53	2	0.9/197
	Low	[0.06–0.22]	$7.1^{+0.6}_{-0.6}$	$1.4^{+0.2}_{-0.1}$	17	0.7	1.0/205
	Very low <sup>d</sup>	<0.06	$3.3^{+0.4}_{-0.0}$	$1.8^{+0.3}_{-0.2}$	1.3	0.04	302.5(99.5)
XTE J1739–302	High	>0.405	$3.7^{+0.5}_{-0.4}$	$0.8^{+0.2}_{-0.1}$	120	1	1.0/160
	Medium	[0.07–0.405]	$3.8^{+0.4}_{-0.4}$	$1.4^{+0.1}_{-0.1}$	18	0.2	0.9/164
	Very low <sup>d</sup>	<0.07	$1.7^{+0.1}_{-0.0}$	$1.4^{+0.2}_{-0.2}$	0.5	0.004	321.9(98.6)
IGR J17544–2619	High	>0.25	$1.9^{+0.3}_{-0.2}$	$1.3^{+0.1}_{-0.1}$	46	0.8	1.0/118
	Medium	[0.07–0.25]	$2.3^{+0.3}_{-0.3}$	$1.7^{+0.2}_{-0.2}$	14	0.3	1.0/108
	Very low <sup>d</sup>	<0.07	$1.1^{+0.1}_{-0.0}$	$2.1^{+0.2}_{-0.2}$	0.2	0.003	183.1(85.1)

<sup>a</sup>Average observed 2–10 keV fluxes in units of  $10^{-12} \text{ erg cm}^{-2} \text{ s}^{-1}$ .

<sup>b</sup>Average 2–10 keV X-ray luminosities in units of  $10^{35} \text{ erg s}^{-1}$  calculated adopting distances determined by Rahoui et al. (2008).

<sup>c</sup>Reduced  $\chi^2$  and d.o.f., or C-stat and percentage of realizations ( $10^4$  trials) with statistic > C-stat.

<sup>d</sup>Fit performed with the constrained column density (see Section 6).

trend down to about 2 counts  $s^{-1}$ . The WT spectrum, extracted during the peak of the outburst (with a grade 0 selection to mitigate residual calibration uncertainties at low energies), results in a hard X-ray emission. When fitted with an absorbed power law, we obtain a photon index of  $1.05^{+0.15}_{-0.14}$  and a column density of  $N_H = (1.3 \pm 0.2) \times 10^{22} \text{ cm}^{-2}$  ( $\chi^2_v = 1.04$  for 104 d.o.f.). The unabsorbed 2–10 keV flux is  $9.5 \times 10^{-10} \text{ erg cm}^{-2} \text{ s}^{-1}$ . The PC spectrum (unabsorbed 2–10 keV flux  $\sim 2 \times 10^{-10} \text{ erg cm}^{-2} \text{ s}^{-1}$ ) fitted with a power-law model yields a photon index of  $1.1 \pm 0.7$  and  $N_H = (1.2^{+1.2}_{-0.8}) \times 10^{22} \text{ cm}^{-2}$  [Cash (1979) statistics and spectra binned to 1 count bin $^{-1}$ ; C-stat = 69.08 for 47 per cent of  $10^4$  Monte Carlo realizations with fitted statistic less than C-stat], consistent with the WT data fit.

BAT mask-weighted spectra were extracted over time-intervals strictly simultaneous with XRT data. We fit the simultaneous BAT+XRT spectra in the time-interval 170–446 s, since the BAT trigger, in the 0.3–10 and 15–150 keV energy bands for XRT and BAT, respectively. Factors were included in the fitting to allow for normalization uncertainties between the two instruments, constrained within their usual ranges (0.9–1.1). Table 7 reports our fits. A simple absorbed power-law model is clearly an inadequate representation of the broad-band spectrum with a  $\chi^2_v = 1.53$  for 117 d.o.f.). We then considered other curved models typically used to describe the X-ray emission from accreting pulsars in HMXBs, such as an absorbed power-law model with a high energy cut-off (HIGHECUT in XSPEC) and an absorbed power-law model with an exponential cut-off (CUTOFFPL). The latter models provide a satisfactory deconvolution of the 0.3–150 keV emission, resulting in a hard power-law-like spectrum below 10 keV, with a roll over of the high energies when simultaneous XRT and BAT data fits are performed. Fig. 7 shows the fits for the CUTOFFPL model.

## 6 OUT-OF-OUTBURST X-RAY SPECTROSCOPY

We characterize the spectral properties of the sources in several states, by accumulating the events in each observation when the source was not in outburst and a detection was achieved. We selected three count rate levels, CR<sub>1</sub>, CR<sub>2</sub> and CR<sub>3</sub> (reported in Table 8), that

would yield comparable statistics in the ranges  $CR_1 < CR < CR_2$  (low),  $CR_2 < CR < CR_3$  (medium) and  $CR > CR_3$  (high). When the statistics did not allow this, we considered only two intensity levels (high and medium). Exposure maps and ARF files were created following the procedure described in Paper V. The spectra were rebinned with a minimum of 20 counts per energy bin to allow  $\chi^2$  fitting. Each spectrum was fitted in the energy range 0.3–10 keV with a single absorbed power law.

We accumulated all data for which no detections were obtained as single exposures (whose combined exposure is  $\Delta T_{\Sigma}$ , reported in Table 5, column 2) and performed a detection. The resulting cu-

mulative mean count rate for each object is reported in Table 5 (column 5). Spectra were also extracted from these event lists. They consisted of  $\sim 200$ – $300$  counts each, so Cash statistics and spectra binned to 1 count  $\text{bin}^{-1}$  were used, instead. When fitting with free parameters, the best-fitting value for  $N_{\text{H}}$  turned out to be consistent with 0, that is, well below the column derived from optical spectroscopy. We therefore performed fits by adopting as a lower limit on the absorbing column the value derived from the Galactic extinction estimate along the line of sight to each source from Rahoui et al. (2008), with a conversion into hydrogen column,  $N_{\text{H}} = 1.79 \times 10^{21} A_V \text{ cm}^{-2}$  (Predehl & Schmitt 1995). Fig. 8 shows

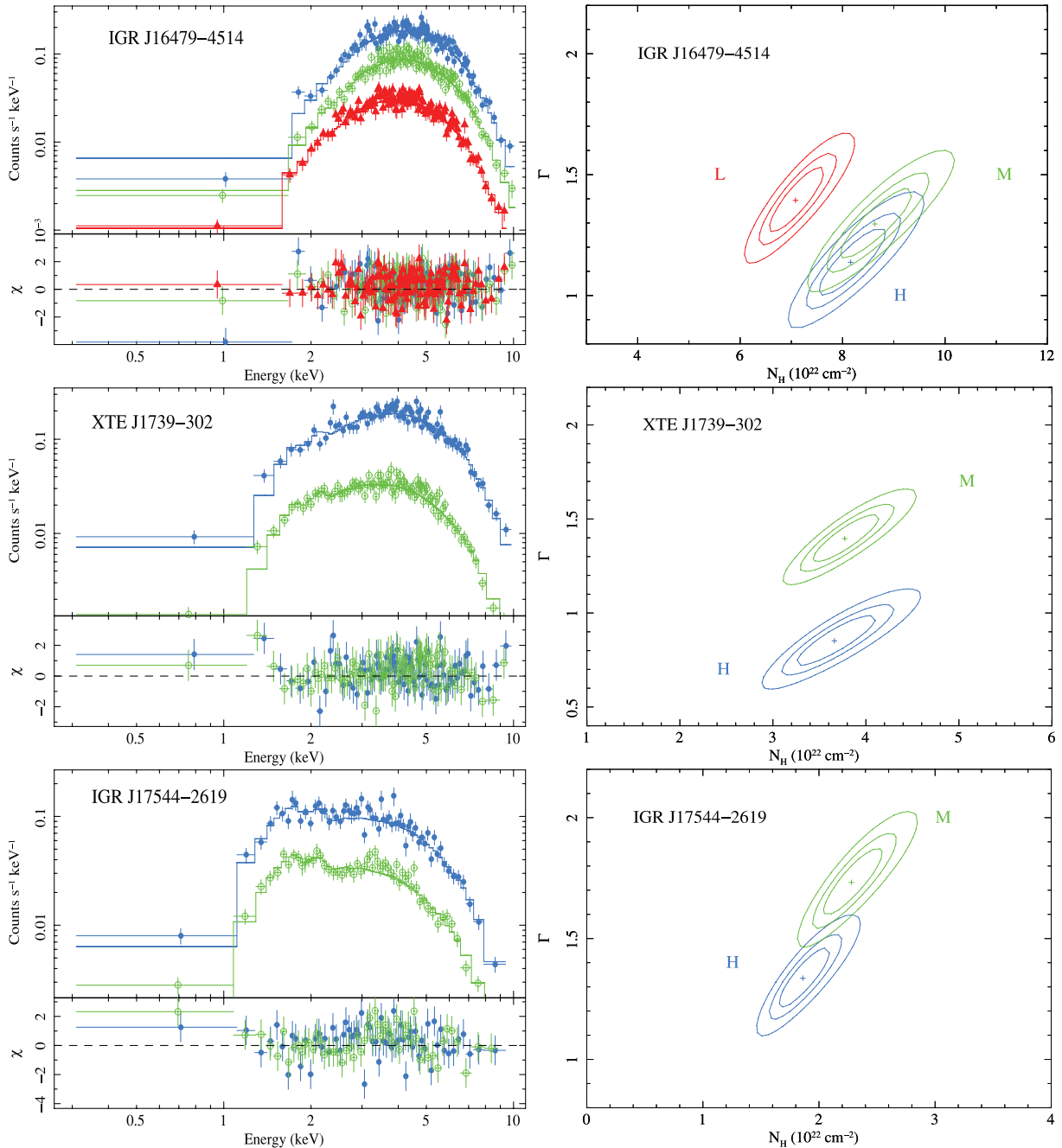


**Figure 8.** Spectroscopy of the 2007–2009 observing campaign. Upper panels (left-hand side): XRT/PC data fitted with an absorbed power law. Lower panels (left-hand side): the residuals of the fit (in units of standard deviations). The filled blue circles, green empty circles and red filled triangles mark high, medium and low states, respectively. Right-hand panels: the  $\Delta\chi^2 = 2.3, 4.61$  and  $9.21$  contour levels for the column density in units of  $10^{22} \text{ cm}^{-2}$  versus the photon index, with best fits indicated by crosses. The labels L, M and H mark low, medium and high states, respectively.

the spectra and contour plots of photon index versus column density; the spectral parameters are reported in Table 8, where we also report the average 2–10 keV luminosities calculated by adopting distances of 4.9 kpc for IGR J16479–4514, 2.7 kpc for XTE J1739–302 and 3.6 kpc for IGR J17544–2619 determined by Rahoui et al. (2008) from optical spectroscopy of the supergiant companions. We also performed fits with an absorbed blackbody, obtaining consistent results with Paper V.

## 7 DISCUSSION

In this paper, we report the results of a monitoring campaign with *Swift* that spans more than a 2-yr baseline. Thanks to the unique characteristics of *Swift*, we can investigate the properties of SFXTs on several time-scales (from minutes to days to years) and in several intensity states (bright flares, intermediate intensity states and down to almost quiescence).

During the second year of monitoring, two different sources flared three times, and in two cases, we obtained multiwavelength observations (see Table 4). XTE J1739–302 triggered the BAT on 2009 March 10. Our results are in general agreement with those obtained during previous outbursts, both in terms of hard photon index and in terms of a relatively lower column density (comparable with the out-of-outburst values). When IGR J17544–2619 triggered the BAT on 2009 June 6, simultaneous BAT and XRT data were collected, thus allowing broad-band spectroscopy. The soft X-ray spectral properties observed during this flare are generally consistent with those observed with *Chandra* [ $\Gamma = 0.73 \pm 0.13$ ,  $N_H = (1.36 \pm 0.22) \times 10^{22} \text{ cm}^{-2}$ , peak flux of  $\sim 3 \times 10^{-9} \text{ erg cm}^{-2} \text{ s}^{-1}$ ; in ‘t Zand 2005]. However, when XRT and BAT data are jointly fitted, an absorbed power-law model is inadequate in fitting the broad-band spectrum, and more curvy models are required. We considered an absorbed power-law model with a high energy cut-off and an absorbed power-law model with an exponential cut-off, models typically used to describe the X-ray emission from accreting neutron stars in HMXBs. We obtained a good deconvolution of the 0.3–150 keV spectrum, characterized by a hard power law below 10 keV and a well-constrained cut-off at higher energies.

In Fig. 9, we compare the light curves of the most recent outbursts of XTE J1739–302 and IGR J17544–2619 (red points) observed by *Swift* during the second year of monitoring, together with the previous outbursts of these sources followed by *Swift*/XRT (grey points). The light curves are referred to their respective BAT triggers (unless the flare did not trigger the BAT, Fig. 9e). The most complete and deep set of X-ray observations of an outburst of an SFXT is the one of the periodic SFXT IGR J11215–5952 (Romano et al. 2007; Sidoli et al. 2007; Romano et al. 2009c), which was instrumental in discovering that the accretion phase during the bright outbursts lasts much longer than a few hours, as seen by lower sensitivity instruments, and contrary to what initially thought at the time of the discovery of this new class of sources (e.g. Sguera et al. 2005). This behaviour is now found to be a common characteristic of the whole sample of SFXTs followed by *Swift*, as our observations on IGR J16479–4514, IGR J08408–4503 and SAX J1818.6–1703 demonstrate (Paper V, Romano et al. 2009a and Sidoli et al. 2009b, respectively); the vertical dashed lines in Fig. 9 mark time-intervals equal to 1 d, up to a week). In the same manner, our observations show that both the large dynamical range (up to 4 orders of magnitude) in flux and a multiple-peaked structure of the light curves of the bright outbursts are equally common characteristics of the sample.

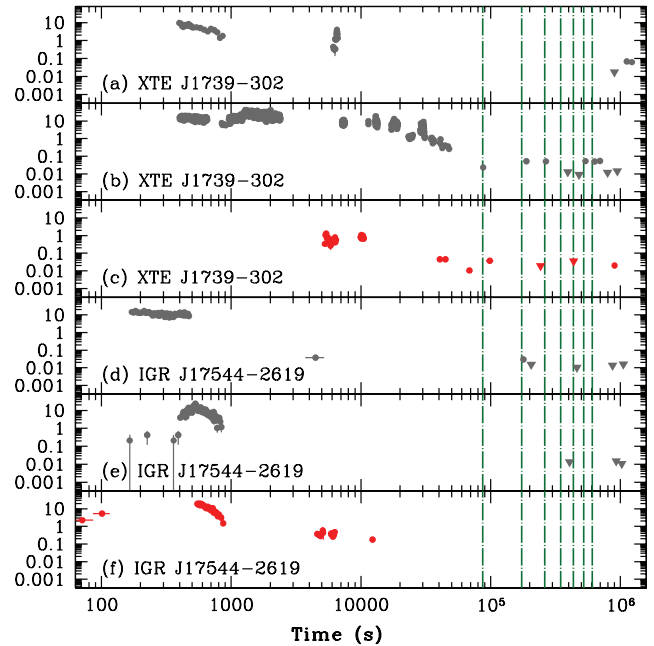


**Figure 9.** Light curves of the outbursts of SFXTs followed by *Swift*/XRT referred to their respective BAT triggers. Points denote detections and triangles denote  $3\sigma$  upper limits. Red data points refer to observations presented here for the first time, while grey data points refer to data presented elsewhere. Note that where no data are plotted, no data were collected. The vertical dashed lines mark time-intervals equal to 1 d, up to a week. Panels (a) and (b) show the flares from XTE J1739–302 (2008-04-08 and 2008-08-13; Paper III and Paper IV, respectively), while panel (c) refers to the 2009 March 10 flare reported here for the first time. Panels (d) and (e) show the flares from IGR J17544–2619 (2008-03-31 and 2008-09-04, Paper III and Paper IV, respectively), while panel (f) refers to the 2009 June 6 flare also reported here for the first time.

In the optical/ultraviolet (UV), we see only marginal variability in the  $u$  and  $uvw1$  magnitudes of XTE J1739–302, and we could exclude a variation of flux corresponding to the X-ray outburst. The  $uvw1$  light curve of IGR J17544–2619 is observed to be remarkably stable. This is consistent with the optical/UV emission being dominated by the constant contribution of the companion stars.

Variability in the X-ray flux is observed at all time-scales and intensity ranges we can probe. Fig. 10 shows, for each of the monitored sources, a montage of time-sequences of the *Swift*/XRT data, where detection was achieved (binned at 100- and 20-s resolutions for PC and WT data, respectively) and with observing and orbital gaps removed from the time-axis. Superimposed on the day-to-day variability (best shown in Fig. 1, which is binned to 1-d resolution) is intraday flaring. As Fig. 10 shows, the latter involves flux variations up to one order of magnitude that can occur down to time-scales as short as an XRT snapshot ( $\lesssim 1$  ks). This remarkable short time-scale variability cannot be accounted for by accretion from a homogeneous wind. On the contrary, it can be naturally explained by the accretion of single clumps composing the donor wind, independently on the detailed geometrical and kinematical properties of the wind and the properties of the accreting compact object. If, for example, we assume that each of these short flares is caused by the accretion of a single clump on to the NS (e.g. in ‘t Zand 2005), then its mass can be estimated (Walter & Zurita Heras 2007) as  $M_{cl} = 7.5 \times 10^{21} (L_{X,36})(t_{fl,3ks})^3 \text{ g}$ , where  $L_{X,36}$  is the average X-ray luminosity in units of  $10^{36} \text{ erg s}^{-1}$  and  $t_{fl,3ks}$  is the duration of the flares in units of 3 ks. We can confidently identify flares down to a

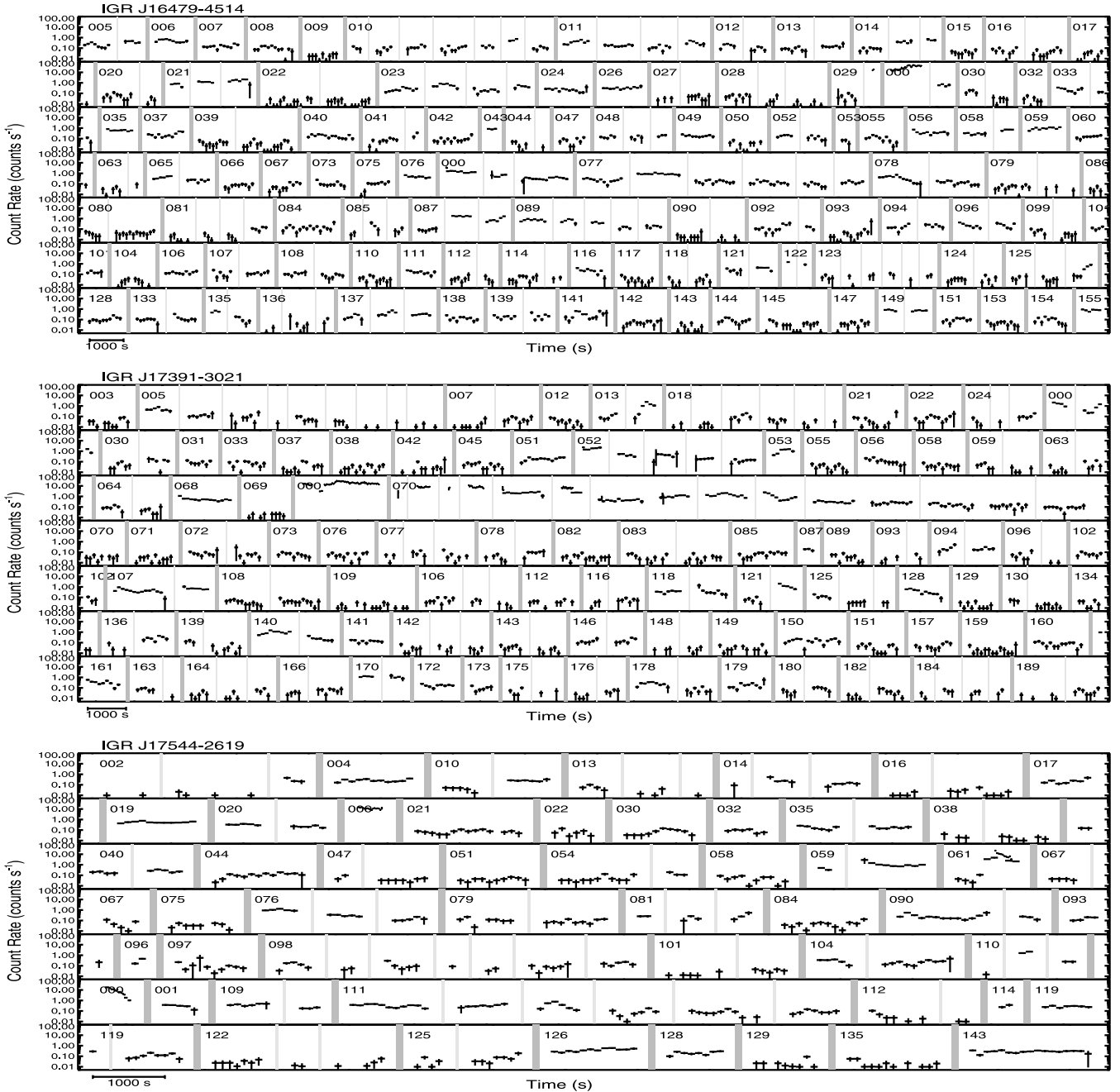


**Figure 10.** *Swift*/XRT (0.2–10 keV) montage of time-sequences. The numbers in the plot identify each observing sequence (see Tables 1–3), with 000 marking outbursts. Non-observing intervals and orbital gaps have been cut out from the time-axis and replaced by thick vertical bars to separate different sequences and by thin grey bars to separate different orbits within each sequence. Each point represents a 100-s bin in PC and a 20-s bin in WT modes. As a reference, in the bottom left, we show the 1000 s time-unit. The light curves are corrected for pile-up PSF losses, vignetting and background-subtracted.

count rate of the order of  $0.1 \text{ counts s}^{-1}$  (within a snapshot of about 1 ks; see Fig. 10); these correspond to luminosities of the order of  $(2\text{--}6) \times 10^{34} \text{ erg s}^{-1}$ , which yield  $M_{\text{cl}} \sim (0.3\text{--}2) \times 10^{19} \text{ g}$ . These masses are about those expected (Walter & Zurita Heras 2007) to be responsible of short flares, below the *INTEGRAL* detection threshold and which, if frequent enough, may significantly contribute to the mass-loss rate.

Our *Swift* monitoring campaign has demonstrated for the first time that X-ray emission from SFXTs is present outside the bright outbursts (Paper I; Paper V), although at a much lower level, thus showing how frequent and typical in SFXTs is accretion at

a low level rate. In this paper, we refined the intensity-selected spectroscopy of the out-of-outburst emission by adopting absorbed power laws, which yield hard power-law photon indices ( $\Gamma \sim 1\text{--}2$ ). All these results are consistent with our findings in Paper V and show that accretion occurs over several orders of magnitude in luminosity (three for XTE J1739–302 and two for the others; Table 8), even when excluding the bright outbursts. In particular, the lowest luminosities we could study with *Swift* are  $4 \times 10^{32}$  and  $3 \times 10^{32} \text{ erg s}^{-1}$  (2–10 keV; ‘very low’ intensity level in Table 8) for XTE J1739–302 and IGR J17544–2619, respectively. These low luminosities are not consistent with Bondi–Hoyle accretion from a spherically

symmetric steady wind (Bondi & Hoyle 1944), as previously reported by Drave et al. (2010) and Clark et al. (2009) for these two SFXTs, thus arguing for a clumpy nature of the accreting wind. This is consistent with our findings on short time-scale variability, which also requires inhomogeneities in the wind.

In the following, we assess the percentage of time each source spends at a given flux state. Fig. 11 shows the distributions of

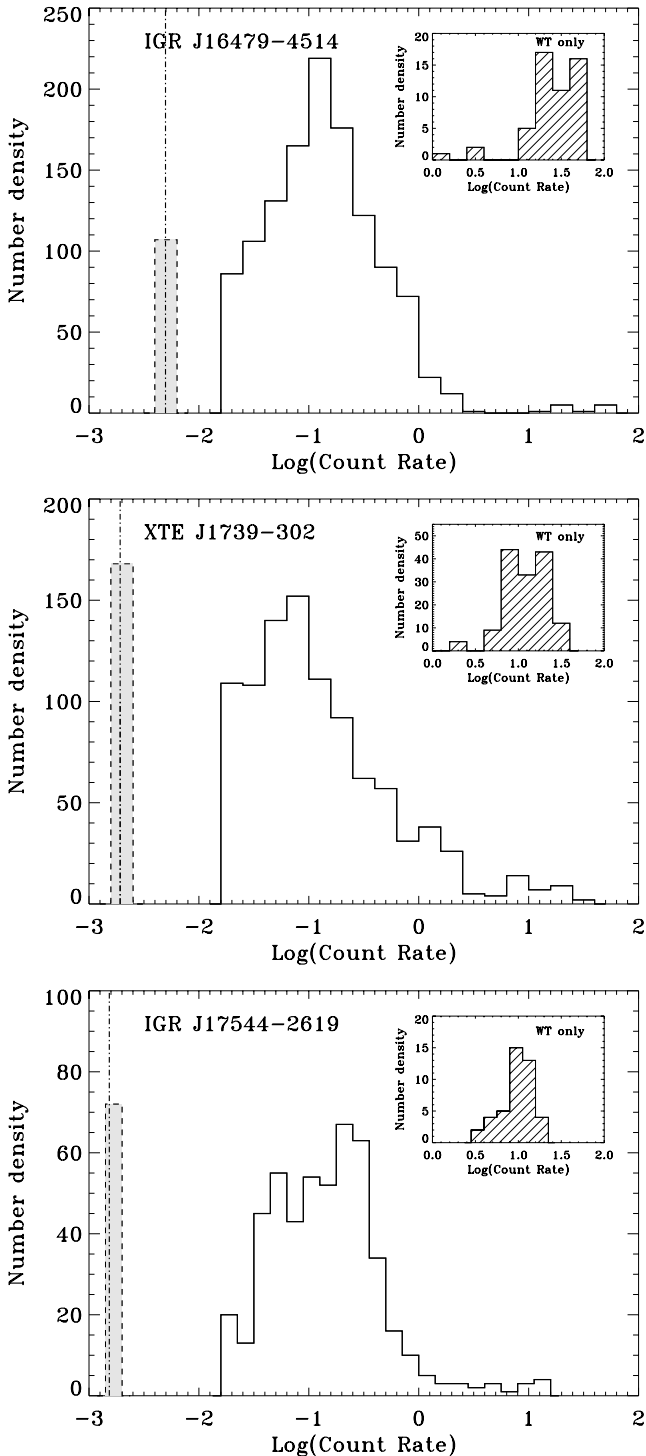


**Figure 11.** Distribution of the count rates when the XRT light curves are binned at 100 s. The vertical lines correspond to the background. The filled histograms are points which are consistent with a zero count rate. The insets show the subset of WT data only, when binned at 20 s.

the observed count rates after removal of the observations where a detection was not achieved (same sample as in Fig. 10, with PC and WT data binned at 100 s). In all cases, a roughly Gaussian shape is observed, with a broad peak at  $\approx 0.1$  counts  $s^{-1}$ , and a clear cut at the detection limit for 100 s at the low end. In particular, when the distributions are fitted with a Gaussian function, we find that their means and  $\sigma$  are 0.12 and 3.4 counts  $s^{-1}$  for IGR J16479–4514; 0.06 and 4.9 counts  $s^{-1}$  for XTE J1739–302; and 0.13 and 3.1 counts  $s^{-1}$  for IGR J17544–2619. This indicates that the most probable flux level at which a random observation will find these sources, when detected, is  $3 \times 10^{-11}$ ,  $9 \times 10^{-12}$  and  $1 \times 10^{-11}$  erg  $cm^{-2}$   $s^{-1}$  (unabsorbed 2–10 keV, obtained using the medium spectra in Table 8), corresponding to luminosities of  $\sim 8 \times 10^{34}$ ,  $8 \times 10^{33}$  and  $2 \times 10^{34}$  erg  $s^{-1}$ , respectively. Fig. 11 also shows the hint of an excess at  $\gtrsim 10$  counts  $s^{-1}$ . Since this count rate is where the WT data of the outbursts are concentrated, we also show them in the insets (dashed histograms) binned at 20-s resolution, which is more appropriate for such count rates. In this case, a clear peak emerges to represent the flaring state of the sources.

We have also calculated the time each source spends *undetected* down to a flux limit of  $(1-3) \times 10^{-12}$  erg  $cm^{-2}$   $s^{-1}$ , and we obtain IDC = 19, 39 and 55 per cent for IGR J16479–4514, XTE J1739–302 and IGR J17544–2619, respectively, with an estimated error of  $\sim 5$  per cent. We note that these values are based on the whole 2-yr campaign, and that the IDC calculated with the observations of 2009 only is 21, 39 and 55 per cent, respectively. These results can be compared with the ones reported in Paper V, where we obtained IDC = 17, 39 and 55 per cent for IGR J16479–4514, XTE J1739–302 and IGR J17544–2619, respectively. We now have a baseline twice as long and almost a factor of 2 higher exposure; the sampling of the light curves has slightly changed during 2009. Nevertheless, the calculated IDC values are remarkably stable, which is indicative of the robustness of this method with respect to the sampling pace.

Considering our monitoring as a casual sampling of the light curve for 2 yr, we can also infer that the time these sources spend in bright outbursts is between 3 and 5 per cent of the total.

## ACKNOWLEDGMENTS

PR dedicates this effort to her grandmother G. Ghedin; she could not follow her aspiration, yet worked hard so that others could. We acknowledge the input from our colleagues along the way during this large project, in particular A. Beardmore, M. M. Chester, L. Ducci, C. Guidorzi, T. Mineo and M. Perri. We thank the *Swift* team duty scientists and science planners. We also thank the remainder of the *Swift* XRT, BAT and UVOT teams, S. Barthelmy and J.A. Nousek in particular, for their invaluable help and support with the planning and execution of the observing strategy. We also thank the anonymous referee for comments that helped improve this paper. This work was supported at PSU by NASA contract NASS-00136. HAK was supported by the *Swift* project.

Facility: *Swift*.

## REFERENCES

- Barthelmy S. D. et al., 2005, *Space Sci. Rev.*, 120, 143
- Blay P. et al., 2008, *A&A*, 489, 669
- Bondi H., Hoyle F., 1944, *MNRAS*, 104, 273
- Bozzo E., Falanga M., Stella L., 2008a, *ApJ*, 683, 1031
- Bozzo E., Stella L., Israel G., Falanga M., Campana S., 2008b, *MNRAS*, 391, L108

- Bozzo E., Giunta A., Stella L., Falanga M., Israel G., Campana S., 2009, *A&A*, 502, 21
- Burrows D. N. et al., 2005, *Space Sci. Rev.*, 120, 165
- Cash W., 1979, *ApJ*, 228, 939
- Clark D. J., Hill A. B., Bird A. J., McBride V. A., Scaringi S., Dean A. J., 2009, *MNRAS*, 399, L113
- Drave S. P., Clark D. J., Bird A. J., McBride V. A., Hill A. B., Sguera V., Scaringi S., Bazzano A., 2010, *MNRAS*, in press (doi:10.1111/j.1365-2966.2010.17383.x) (arXiv:1007.3379)
- Grebenev S. A., Lutovinov A. A., Sunyaev R. A., 2003, *Astron. Tel.*, 192
- Grebenev S. A., Rodriguez J., Westergaard N. J., Sunyaev R. A., Oosterbroek T., 2004, *Astron. Tel.*, 252
- in 't Zand J. J. M., 2005, *A&A*, 441, L1
- in 't Zand J., Heise J., Ubertaini P., Bazzano A., Markwardt C., 2004, in Schoenfelder V., Lichti G., Winkler C., eds, *ESA SP-552, 5th INTEGRAL Workshop on the INTEGRAL Universe*. ESA, Noordwijk, p. 427
- Jain C., Paul B., Dutta A., 2009, *MNRAS*, 397, L11
- Kennea J. A., Pagani C., Markwardt C., Blustin A., Cummings J., Nousek J., Gehrels N., 2005, *Astron. Tel.*, 599
- Krimm H. et al., 2006, *Astron. Tel.*, 904
- Krimm H. A. et al., 2007, *Astron. Tel.*, 1265
- Krimm H. A., Barthelmy S. D., Cummings J. R., Markwardt C. B., Skinner G., Tueller J., Swift/BAT Team, 2008, in *AAS/High Energy Astrophys. Div. Vol. 10. Am. Astron. Soc., Los Angeles*, p. #07.01
- Krimm H. A., Romano P., Sidoli L., 2009, *Astron. Tel.*, 1971
- Kuulkers E. et al., 2007, *Astron. Tel.*, 1266
- La Parola V. et al., 2009, *Astron. Tel.*, 1929
- Markwardt C. B., Krimm H. A., 2006, *Astron. Tel.*, 816
- Molkov S., Mowlavi N., Goldwurm A., Strong A., Lund N., Paul J., Oosterbroek T., 2003, *Astron. Tel.*, 176
- Negueruela I., Smith D. M., Harrison T. E., Torrejón J. M., 2006, *ApJ*, 638, 982
- Negueruela I., Torrejón J. M., Reig P., Ribó M., Smith D. M., 2008, in Bandyopadhyay R. M., Wachter S., Gelino D., Gelino C. R., eds, *AIP Conf. Ser. Vol. 1010, A Population Explosion: The Nature & Evolution of X-ray Binaries in Diverse Environments*. Am. Inst. Phys., New York, p. 252
- Pellizza L. J., Chaty S., Negueruela I., 2006, *A&A*, 455, 653
- Poole T. S. et al., 2008, *MNRAS*, 383, 627
- Predehl P., Schmitt J. H. M. M., 1995, *A&A*, 293, 889
- Rahoui F., Chaty S., Lagage P.-O., Pantin E., 2008, *A&A*, 484, 801
- Rampy R. A., Smith D. M., Negueruela I., 2009, *ApJ*, 707, 243
- Romano P., Sidoli L., Mangano V., Mereghetti S., Cusumano G., 2007, *A&A*, 469, L5
- Romano P. et al., 2008a, *Astron. Tel.*, 1697
- Romano P. et al., 2008b, *Astron. Tel.*, 1659
- Romano P. et al., 2008c, *Astron. Tel.*, 1466
- Romano P. et al., 2008d, *ApJ*, 680, L137 (Paper II)
- Romano P. et al., 2009a, *MNRAS*, 392, 45
- Romano P. et al., 2009b, *MNRAS*, 399, 2021 (Paper V)
- Romano P., Sidoli L., Cusumano G., Vercellone S., Mangano V., Krimm H. A., 2009c, *ApJ*, 696, 2068
- Romano P. et al., 2009d, *Astron. Tel.*, 1961
- Romano P. et al., 2009e, *Astron. Tel.*, 1920
- Romano P. et al., 2009f, *Astron. Tel.*, 2069
- Roming P. W. A. et al., 2005, *Space Sci. Rev.*, 120, 95
- Sguera V. et al., 2005, *A&A*, 444, 221
- Sguera V. et al., 2006, *ApJ*, 646, 452
- Sidoli L., Paizis A., Mereghetti S., 2006, *A&A*, 450, L9
- Sidoli L., Romano P., Mereghetti S., Paizis A., Vercellone S., Mangano V., Götz D., 2007, *A&A*, 476, 1307
- Sidoli L. et al., 2008a, *Astron. Tel.*, 1454
- Sidoli L. et al., 2008b, *ApJ*, 687, 1230 (Paper I)
- Sidoli L. et al., 2009a, *MNRAS*, 397, 1528 (Paper IV)
- Sidoli L. et al., 2009b, *MNRAS*, 400, 258
- Sidoli L. et al., 2009c, *ApJ*, 690, 120 (Paper III)
- Smith D. M., Main D., Marshall F., Swank J., Heindl W. A., Leventhal M., in 't Zand J. J. M., Heise J., 1998, *ApJ*, 501, L181
- Sunyaev R. A., Grebenev S. A., Lutovinov A. A., Rodriguez J., Mereghetti S., Gotz D., Courvoisier T., 2003, *Astron. Tel.*, 190
- Vaughan S. et al., 2006, *ApJ*, 638, 920
- Walter R., Zurita Heras J., 2007, *A&A*, 476, 335
- Walter R. et al., 2006, *A&A*, 453, 133

## SUPPORTING INFORMATION

Additional Supporting Information may be found in the online version of this paper:

**Table 1.** Observation log for IGR J16479–4514.

**Table 2.** Observation log for IGR J17391–3021.

**Table 3.** Observation log for IGR J17544–2619.

Please note: Wiley-Blackwell are not responsible for the content or functionality of any supporting materials supplied by the authors. Any queries (other than missing material) should be directed to the corresponding author for the article.

This paper has been typeset from a  $\text{\TeX}/\text{\LaTeX}$  file prepared by the author.